Title

Thermal plasma and fast ion transport in electrostatic turbulence in the large plasma devicea)

Journal

Physics of Plasmas, 19(5)

ISSN

1070-664X

Authors

Zhou, Shu

Heidbrink, WW

Boehmer, H

et al.

Publication Date

2012-05-01

DOI

10.1063/1.3695341

Thermal plasma and fast ion transport in electrostatic turbulence in the large plasma device[a)]

Shu Zhou,[1,b)] W. W. Heidbrink,[1] H. Boehmer,[1] R. McWilliams,[1] T. A. Carter,[2] S. Vincena,[2] S. K. P. Tripathi,[2] and B. Van Compernolle[2]
[1]*Department of Physics and Astronomy, University of California, Irvine, California 92697, USA*
[2]*Department of Physics and Astronomy, University of California, Los Angeles, California 90095, USA*

(Received 30 November 2011; accepted 1 March 2012; published online 28 March 2012)

The transport of thermal plasma and fast ions in electrostatic microturbulence is studied. Strong density and potential fluctuations ($\delta n/n \sim \delta\phi/kT_e \sim 0.5$, f ~ 5–50 kHz) are observed in the large plasma device (LAPD) [W. Gekelman, H. Pfister, Z. Lucky *et al.*, Rev. Sci. Instrum. **62**, 2875 (1991)] in density gradient regions produced by obstacles with slab or cylindrical geometry. Wave characteristics and the associated plasma transport are modified by driving sheared E × B drift through biasing the obstacle and by modification of the axial magnetic fields (B_z) and the plasma species. Cross-field plasma transport is suppressed with small bias and large B_z and is enhanced with large bias and small B_z. The transition in thermal plasma confinement is well explained by the cross-phase between density and potential fluctuations. Large gyroradius lithium fast ion beam ($\rho_{fast}/\rho_s \sim 10$) orbits through the turbulent region. Scans with a collimated analyzer give detailed profiles of the fast ion spatial-temporal distribution. Fast-ion transport decreases rapidly with increasing fast-ion energy and gyroradius. Background waves with different scale lengths also alter the fast ion transport. Experimental results agree well with gyro-averaging theory. When the fast ion interacts with the wave for most of a wave period, a transition from super-diffusive to sub-diffusive transport is observed, as predicted by diffusion theory. Besides turbulent-wave-induced fast-ion transport, the static radial electric field (E_r) from biasing the obstacle leads to drift of the fast-ion beam centroid. The drift and broadening of the beam due to static E_r are evaluated both analytically and numerically. Simulation results indicate that the E_r induced transport is predominately convective. © *2012 American Institute of Physics*. [http://dx.doi.org/10.1063/1.3695341]

I. INTRODUCTION

Plasma transport in turbulent waves is very important both in fusion experiments and in space physics. Specifically, reduction of the cross-field transport by modification of the turbulence at the plasma edge has attracted growing interest since the discovery of the so-called high confinement mode[1] (H-mode) in magnetic confinement devices. Many experiments and theories attribute the reduction in plasma transport to the development of velocity shear at the plasma edge. The sheared flow in plasmas can be spontaneously generated by nonlinear interaction of the edge turbulence (zonal flows, see Ref. 2 and references therein) or induced by radial electric fields (E × B drift, see Refs. 3 and 4, and references therein). It is demonstrated[5] that the E × B drift induced by external bias can also trigger an H-mode like state in plasma. The mechanism of this confinement transition has been further studied in experiments.[6–9]

Another important topic in turbulent transport is the transport of energetic ions in microturbulence. Energetic ions are defined as ions with much higher energy than the plasma thermal ions. Experimental results reported in tokamaks indicates that, in the high energy regime (the ratio of fast ion energy to thermal ion energy $E_{fast}/T_i \gg 10$), ions are well confined in electrostatic microturbulence (see, e.g., Ref. 10 and references therein). But anomalous transport at small E_{fast}/T_i has been reported.[11–17] It is widely accepted that the reduction of the energetic ion transport in microturbulence is due to the averaging effect of its large gyro and drift orbit over the turbulent structures with a scale length of thermal ion gyro-radius (ρ_i). Many theoretical and simulation works (e. g., Refs. 18 and 19) have been performed to model this gyro-averaging effect, but experimental results are rarely reported.

Two experiments have been performed at the large plasma device[20] (LAPD) to study the transport of both thermal plasma and fast ions in electrostatic turbulent waves. An obstacle is inserted in the main plasma column to partially block the plasma source and induces a sharp gradient in plasma density. Biasing the obstacle induces sheared E × B flow at the plasma edge. The turbulent waves are driven by both density gradient and sheared flow. The plasma transport and confinement are effectively modified by control parameters such as the bias voltage on the obstacle (V_{bias}) and strength of the axial magnetic field (B_z). The confinement of the plasma density is either improved or weakened depending on the control parameters. The transition in density confinement is found to correlate with the phase overlap between fluctuating density and potential structures.

The turbulent waves also serve as the background wave fields for the fast-ion transport studies. A fast-ion source[21] is

[a)]Paper GI3 3, Bull. Am. Phys. Soc. **56**, 95 (2011).
[b)]Invited speaker.

inserted in the LAPD as a test-particle beam, and the electrostatic fluctuations cause the beam width to broaden. Fast-ion transport in electrostatic waves with various spatial-temporal characteristics is documented. The energy scaling of the transport and the scaling on the structure size and correlation length of the background waves are consistent with theoretical predictions.

This paper summarizes the main results reported in earlier publications about the thermal[22] and fast-ion[23,24] transport in these LAPD experiments. It also includes new material on a possible source of uncertainty in the fast-ion transport experiment: the effect of the static electric field on the fast ion beam. The experimental setup is introduced in Sec. II. The results of the thermal plasma and fast-ion transport in electrostatic turbulent waves are briefly reviewed in Secs. III and IV. Section V discusses the effect of the bias-induced static electric field on the measured drift and broadening of the fast-ion beam. Conclusions are drawn in Sec. VI.

II. EXPERIMENTAL SETUP

The experiments reported in this paper are performed in the upgraded LAPD at the University of California, Los Angeles (UCLA). LAPD is an 18-m-long, 1-m-diameter cylindrical vacuum chamber, coaxial with 56 solenoid magnetic field coils. The axial magnetic field in this experiment is uniform with $B_z \sim 600\,\text{G}$–$1800\,\text{G}$. Pulsed plasmas with $\sim$10 ms duration are created using a barium oxide coated cathode source at 1 Hz repetition rate. During the pulse time, a 40–60 V bias is applied between the cathode and anode, resulting in $\sim$4 kA of discharge current. Primary electrons with energy comparable to the cathode-anode bias voltage are generated during the discharge. These primary electrons flow downstream along the axial magnetic field lines and lead to ionization in the main chamber. The plasma column has a diameter of $\leq$70 cm. The working gases used in this experiment are helium and neon. Typical parameters during the active discharge in a helium plasma (at a fill pressure of $\sim 2 \times 10^{-4}$ Torr) are $n_e \sim 2.5 \times 10^{12}\,\text{cm}^{-3}$, $T_e \sim 5\,\text{eV}$, and $T_i \sim 1\,\text{eV}$. The experimental setup is shown schematically in Fig. 1. A copper, annular obstacle with inner diameter of 12 cm and outer diameter of 20 cm is inserted upstream (port 29), concentrically with the plasma column. Once in place, the obstacle blocks the plasma-forming primary electrons parallel to the magnetic field and significantly decreases the downstream plasma density. A steep density gradient, along with large density fluctuations, is observed on the inner edge region of the annular depletion. The annular obstacle is either floating or positively biased relative to the LAPD anode. The obstacle shaft and the LAPD anode are connected by a bias circuit that contains a capacitor bank and an insulated gate bipolar transistor (IGBT) switch. A pulsed bias with $\sim$3 ms duration time can be imposed on the obstacle during the steady portion of the LAPD discharge. The biasing voltage is up to 250 V, and it establishes radial electric fields and spins the edge of the 12 cm-diameter plasma column through the $E \times B$ drift. Measurements of plasma density, floating potential, temperature, and their fluctuations are made using Langmuir probes.[25]

The lithium ion gun[21] is inserted into the LAPD plasma at port 35 with variable pitch angle to the axial magnetic field. The initial width of the lithium ion beam is limited by the exit aperture of the gun ($\sim$5 mm), while the beam energy is set by the biasing voltage between the lithium emitter and the molybdenum grid on the aperture. The fast ion energy in this experiment ranges from 300 eV to 1000 eV. The angular divergence of the beam is $\sim\pm 5^\circ$, with energy divergence $\sim$5 eV. The ion beam trajectories are helical: parallel motion along the magnetic field with nearly constant velocity v_z and gyro motion perpendicular to the magnetic field. The beam trajectories fully overlap with large plasma density and potential fluctuations. A collimated fast ion collector is inserted at four axial locations (port 30–33, with axial

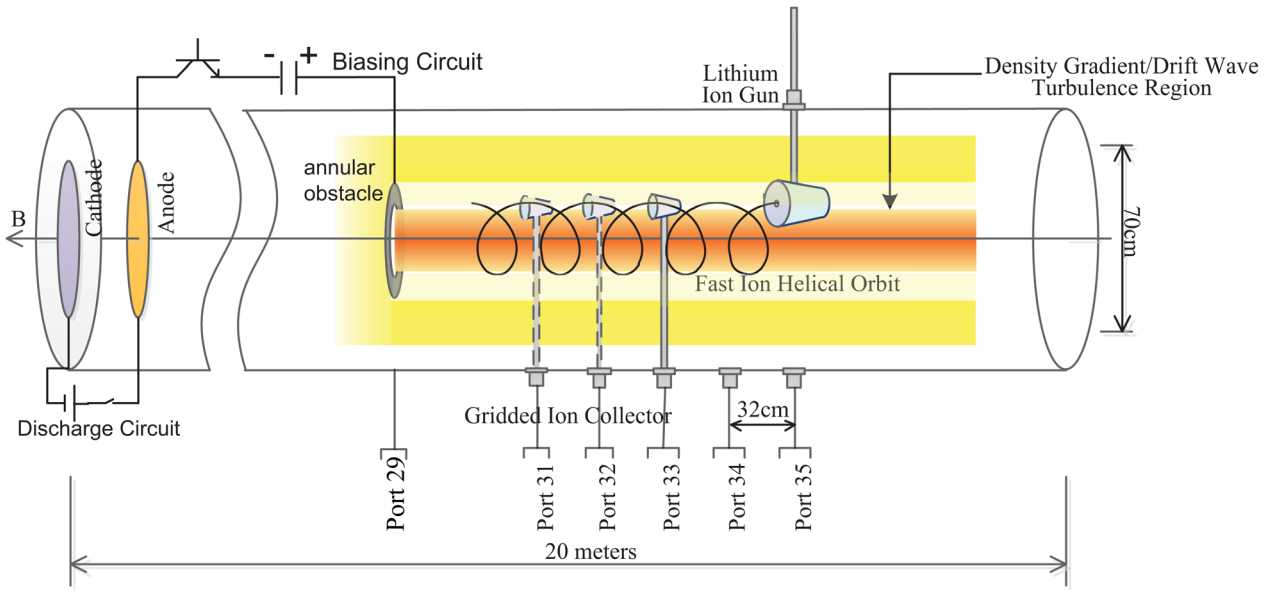

FIG. 1. Schematic of the experimental setup in the LAPD.

distance of 64–160 cm from the source) to measure the beam spreading as a function of its time-of-flight in the waves.

III. CONFINEMENT TRANSITION OF THERMAL PLASMAS

The confinement transition of the central plasma column (with diameter ~12 cm) under this experimental setup is described in detail in Ref. 22. The major results are summarized here. Transport of the thermal plasma is modified by two control parameters: bias voltage on the obstacle (V_{bias}, ranges from 25 V to 250 V) and axial magnetic field strength (B_z, ranges from 600 G to 1800 G). In addition, transport behavior is also different with helium or neon plasmas. The evolution of the plasma density during the obstacle-biasing time in all experimental cases can be categorized into two phenomena: improved confinement (Fig. 2(b)) or density depletion (Fig. 2(c)). Cases with improved confinement feature an increase in plasma density during the pulsed bias and steepening of the density gradient at the plasma edge. In cases with density depletion, a large decrease in plasma density is always observed. An empirical study of all experimental cases (Fig. 2(a)) indicates that the transition between improved confinement and plasma depletion is related to both the E × B drift velocity ($V_{E\times B}$) induced by external bias and the scale length of the ion sound radius (ρ_s). Cases with improved confinement are associated with small $V_{E\times B}$ and small ρ_s, while cases with density depletion are associated with large $V_{E\times B}$ and large ρ_s.

The mechanism of the difference in plasma cross-field transport and confinement is understood. The radial density flux profiles are calculated to show directly the radial transport of the plasma density. Figures 3(a) and 3(b) show the radial flux profiles for typical cases of improved confinement (a) and density depletion (b). Figures 3(c) and 3(d) show the associated structures of the density (filled contour) and potential (line contour) fluctuations, represented by the cross-correlation functions of the ion saturation current ($\tilde{I}_{sat}$) and floating potential ($\tilde{V}_f$). In the case with improved confinement, a reversal in the direction of the radial flux is observed at the plasma edge (r ~ 6 cm). The reversal occurs in the region with the large sheared E × B velocity that is induced by the obstacle bias. The overlap of $\tilde{I}_{sat}$ and $\tilde{V}_f$ structures (Fig. 3(c)) in this case shows that the sheared structures cause a reversal of the cross-phase, which is consistent with the radial flux profile. In the case with density depletion, the radial flux is dominated by outward transport (Fig. 3(b)) and the fluctuations of $\tilde{I}_{sat}$ and $\tilde{V}_f$ are dominated by m = 1 modes with long radial extension in the structure (Fig. 3(d)). This is also consistent with the depletion of the plasma density in these cases.

IV. FAST ION TRANSPORT IN ELECTROSTATIC WAVES

The turbulent waves induced by obstacles provide a good environment to study the transport of the fast ions in electrostatic microturbulence. A test-particle lithium ion beam is introduced into the LAPD chamber (see Fig. 1). The fast-ion beam orbit is designed to overlap partially or fully with the turbulent wave fields, and the position and radial broadening of the collected beam spots indicate transport due to wave-particle interaction. Figures 4(a)–4(d) summarize the wave structures and fast-ion orbits in four typical cases. Fluctuations in Fig. 4(a) are induced by a half-plate obstacle,[26] while fluctuations in Figs. 4(b)–4(d) are induced by the annular obstacle described in Sec. II. With a half-plate obstacle, the fast ion transport as a function of the fast ion energy and gyro-radius is studied.[23] Following Eq. (6) in Ref. 23, the turbulent wave induced fast ion transport is quantified by $(W^2 - W^2_{classical})$, where W is the radial full-width at half-maximum (FWHM) of the collected beam. Figure 5 shows the energy dependence of the wave-induced fast ion transport. It is observed that the beam transport is nearly classical at high energy (~1000 eV). At low energy

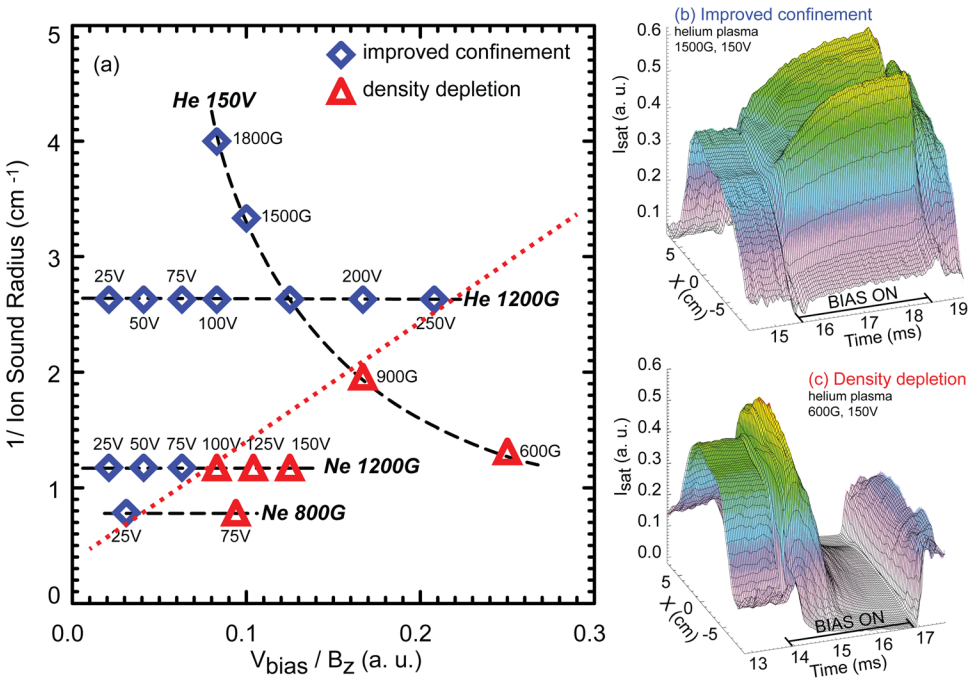

FIG. 2. (a) Plot of all cases studied with control parameters marked. Horizontal axis indicates the direction of increasing flow velocity; vertical axis indicates the direction of decreasing ion sound radius (ρ_s). Dotted line is drawn to guide the eye. Cases with large radial transport and plasma depletion tend to be associated with large flow velocity and large ρ_s. (b) Spatial-temporal evolution of I_{sat} signal for a case with improved confinement. (c) Spatial-temporal evolution of I_{sat} signal for a case with density depletion.

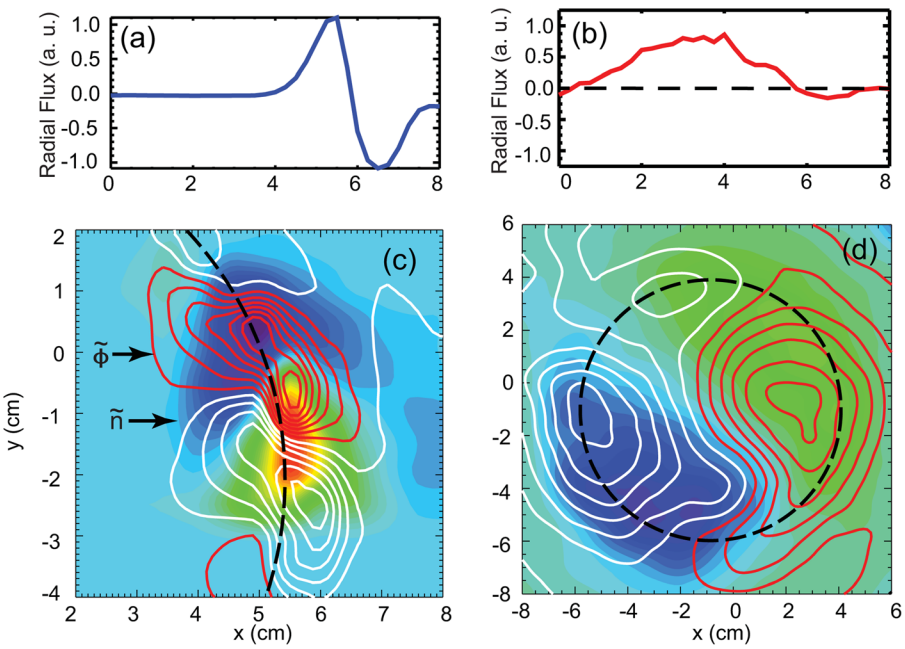

FIG. 3. Upper panel: radial flux profiles for typical (a) improved confinement and (b) density depletion cases. Lower panel: density fluctuation (filled contour) and potential fluctuation (line contour) structures in cases with (c) improved confinement and (d) density depletion.

(~400 eV), the wave induced transport dominates the broadening of the beam. This result is well explained by the so called gyro-averaging effect, which states that the effective turbulent field sampled by a particle is averaged over the particle gyro-orbit. Detailed discussion on this experiment can be found in Ref. 23 and references therein.

Three cases with the annular obstacle (Figs. 4(b)–4(d)) further study the dependence gyro-averaging effects on the characteristics of the background turbulent waves. With different control parameters (see Sec. III), three cases with different wave correlation lengths (L_{corr}) and structure sizes (L_s) are observed, and the fast-ion beam transport under these cases is compared. L_{corr} is defined as the azimuthal scale length of the correlated wave structures, while L_s is defined as the scale length of a single eddy structure. For this study, the fast ion energy and orbit size is kept constant. Figure 6 shows that large wave-induced transport is observed in background waves with large L_s. In two cases with similar L_s, turbulent waves (with short L_{corr}) induce more fast-ion transport than coherent waves (with long L_{corr}). The experimental observations are explained by the effectiveness of gyro-averaging in these cases.[24] The time dependence of the fast ion transport is also studied. In theory, the nature of the beam transport in waves can be described[19] as super-diffusive, sub-diffusive, or diffusive depending on the time scale of the wave-particle interaction. In the experiment, it is observed (Fig. 7) that, when the fast ion time-of-flight in the wave is shorter than any of the wave time scales, the

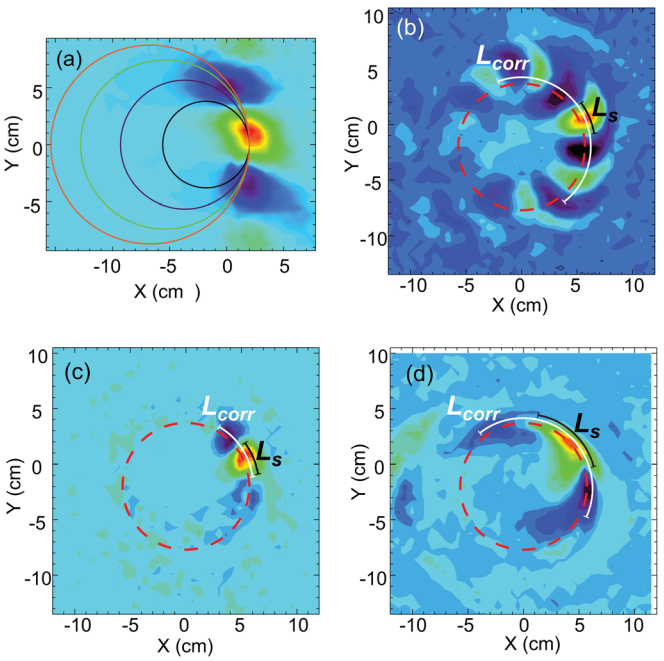

FIG. 4. Turbulent wave fields (represented by the cross-correlation function of I_{sat}) and associated fast ion orbits in four cases. A half-plate obstacle is used in case (a), while an annular obstacle is used in case (b)–(d).

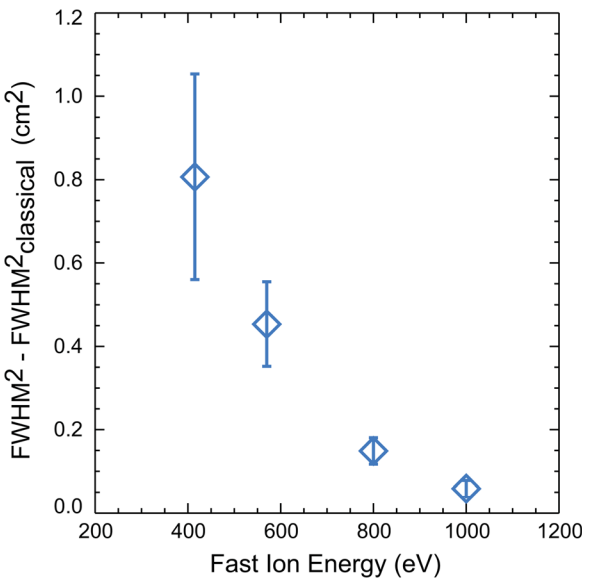

FIG. 5. Wave induced broadening of the beam width as a function of the fast ion energy, with the background waves shown in Fig. 4(a).

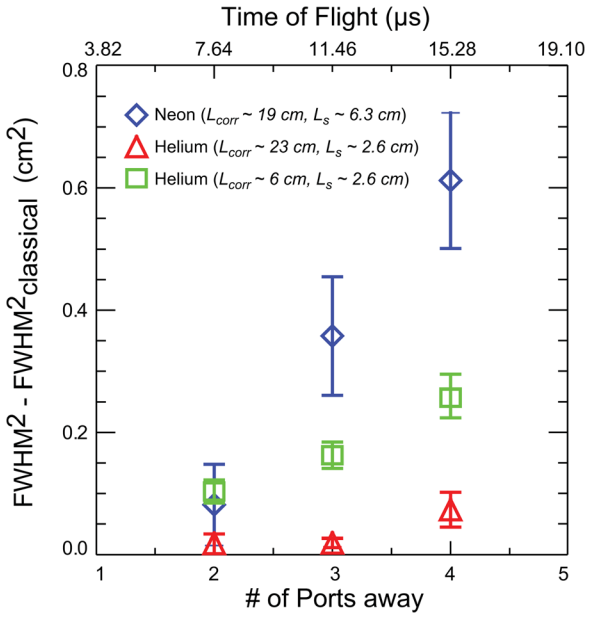

FIG. 6. Wave induced broadening of the beam width in three cases with different wave spatial scales (Figs. 4(b)–4(d)).

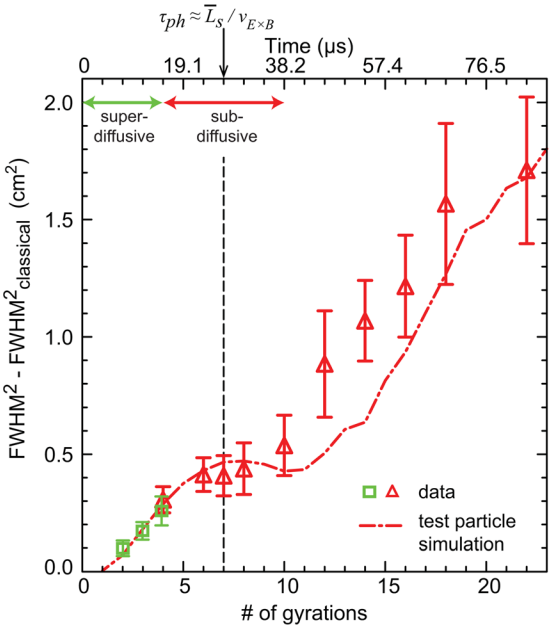

FIG. 7. Spatial-temporal evolution of the fast-ion beam width versus number of gyro-orbits. A test-particle simulation result (red dashed-dotted line) agrees well with the data.

transport is super-diffusive, with the beam diffusion coefficient growing linearly with time ($D_\perp \propto t$, $W^2 - W^2_{classical} \sim t^2$); when the fast ion time-of-flight in the wave is comparable to the time scale of the wave phase changing ($\tau_{ph} \approx \bar{L}_s / V_{E\times B}$), the transport is sub-diffusive, with the slope of ($W^2 - W^2_{classical}$) decreasing with time. A test particle Monte-Carlo simulation is performed to model the fast-ion diffusion using the experimentally measured wave fields. The simulation result (red dashed line in Fig. 7) agrees well with the data. Detailed discussion of the dependence of fast ion transport on the nature of the turbulence can be found in Ref. 24 and references therein.

V. EFFECTS OF STATIC ELECTRIC FIELDS ON THE FAST ION BEAM

In this experimental setup, besides the interaction of the fast-ion beam with the turbulent wave fields, the fast ions are also affected by the static radial electric fields (E_r) induced by the bias on the annular obstacle. The fast ion beam gyro radius ($\rho_f = 5.7$ cm) is set to be smaller than the inner radius of the annular obstacle (~6 cm). The fast ion beam trajectory mainly interacts with the potential structures ($L_{\tilde{\phi}} \sim 5$ cm), while also under the effect of the static potential gradient (with a scale size $L_{\nabla\phi} \sim 0.5$ cm). The observed effect of the radial static electric fields on the fast-ion beam is mainly a convective drift of the beam center. Figure 8(a) shows the beam profiles collected 2 ports away from the source in helium plasmas when the bias on the obstacle is either off or on ($V_{bias} = 100$ V). It is observed that, during the pulse-bias time, the center of the beam drifts in the −r direction, with a displacement of ~5 mm.

Drifting of the centroid is often observed. These drifts occur both in time (in a single discharge as plasma conditions change) and in space (at the same time in the discharge at different distances from the source). Empirically, the magnitude of the drift tends to increase with increasing annulus bias and with increasing distance from the source (Fig. 8(b)). In general, both radial and azimuthal drifts are observed.

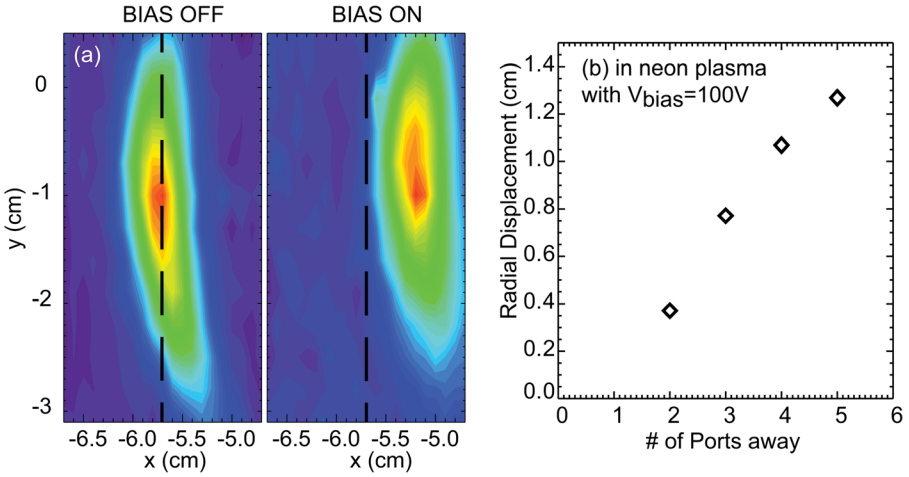

FIG. 8. (a) Observed radial displacement of a fast-ion beam profile 2 ports away from the ion source during the bias time ($V_{bias} = 100$ V) of the obstacle in helium plasma. (b) Radial displacement of the beam center versus the distance from the source in neon plasma with $V_{bias} = 100$ V.

The direction and magnitude of the drift are sensitive to the alignment of the orbit relative to the annulus. Motion of the centroid also can occur in the absence of a biased plate. For example, the beam centroid often moves ~5 mm at the transition between the active phase of the discharge and the afterglow phase. The jump at this transition is sensitive to the electrical configuration of the ion source housing, with a different response depending on whether the gun is floating or grounded. All of these phenomena are consistent with the idea that static electric fields cause convective drifts.

The effect of a static E_r fields on the fast ion orbits can be studied analytically. Assuming the radial displacement of the ion $\delta r \ll \rho$, where ρ is the gyroradius of the fast ion, the equation of motion of a single fast ion is

$$m\frac{d^2\vec{r}}{dt^2} = q(\vec{E} + \vec{v} \times \vec{B}), \text{ with } \vec{r} = \vec{\rho} + \delta\vec{r}, \omega = \Omega + \delta\omega.$$

Here Ω is the fast-ion gyro frequency and ω is the actual angular velocity. Consider the case of an orbit that is concentric with a biased annulus. By symmetry, the electric field is only in the radial direction, thus $E_\theta = 0$. The equation of motion in the radial direction is

$$\delta\ddot{r} = \frac{e}{m}E_r - \Omega^2\delta r. \quad (5.1)$$

If E_r is a constant, the equation has a simple analytical solution of the form

$$\delta r = (eE_r/m\Omega^2) + A\sin(\Omega t + \varphi),$$

which is a sinusoidal oscillation at the fast ion gyro frequency. For a more complicated electric field, such as the experimental plasma potential and E_r profiles during the bias time, a numerical solution of Eq. (5.1) can be derived.

Figure 9 shows the numerical solution of the fast-ion radial displacement as a function of time under the measured equilibrium plasma potential with 75 V obstacle-bias voltage in neon plasmas. The red dashed lines mark the end time of each fast-ion cyclotron motion. As the experimental profile of E_r is non-uniform, the radial oscillation frequency of the fast ion diverges from the cyclotron frequency Ω. The

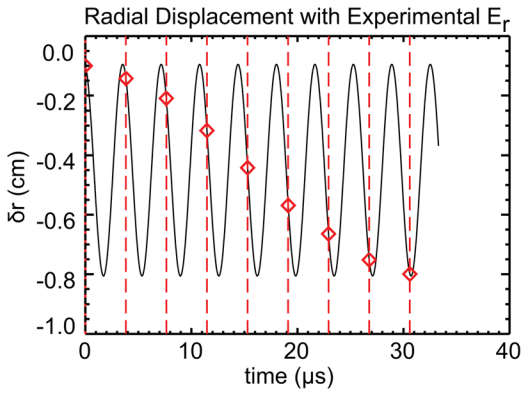

FIG. 9. Numerical solution of the particle radial displacement under the effect of the static radial electric field. Red diamonds are the particle radial displacement at the end of each cyclotron motion.

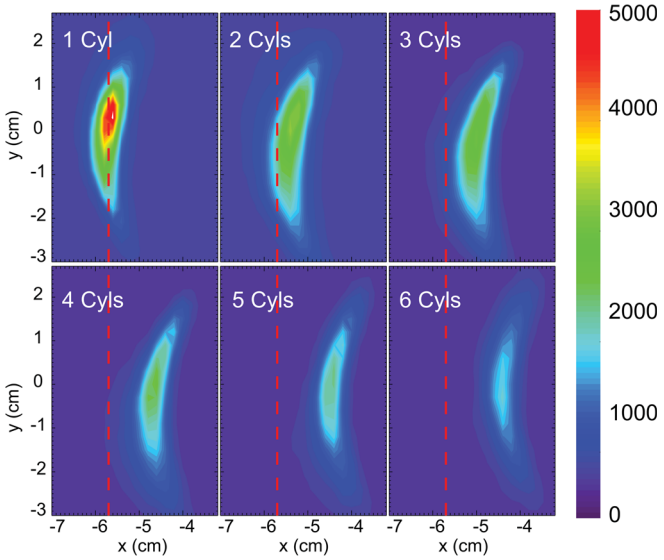

FIG. 10. Radial drift of the collected beam profiles at 1–6 gyrations, observed in a Monte-Carlo simulation with experimental profile of plasma potential and 50 000 test particles.

displacement of the fast ion in the −r direction at the end of each cyclotron motion increases with the number of gyrations. This indicates that the radial motion of the particle is precessing in these non-uniform electric fields. This result agrees with the observed tendency of the drift to increase approximately linearly with distance from the source (Fig. 8(b)). The numerically solved displacement scale length (~1 cm) also agrees with the observation.

Due to the finite radial width of the fast-ion beam and the non-uniform fields, not all particles experience the same drift. Hence, the collective effect of the static electric fields on the beam spot is not fully convective. Broadening of the beam radial FWHM can result from the static fields as well. This is a source of error in the study of beam broadening due to the turbulent waves. To evaluate the effect of the static fields on the beam FWHM, a Monte-Carlo simulation is performed. Equilibrium profiles of plasma potential in an experimental case (neon plasma with 75 V bias) are imported to a Monte-Carlo particle following code as the background

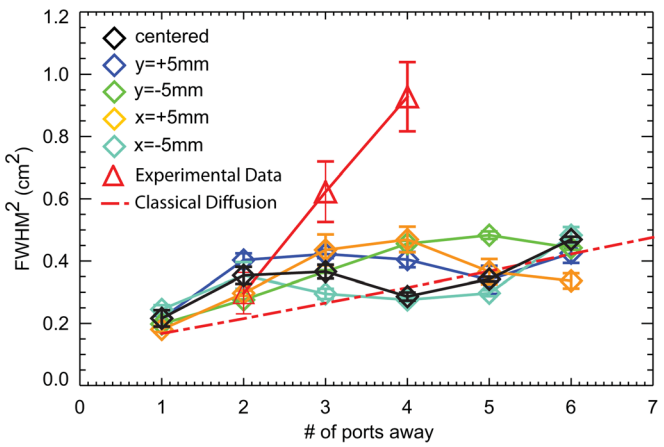

FIG. 11. Simulated broadening of the beam FWHM due to the static radial electric fields. The observed beam width (triangles) and classical diffusion level (dashed-dotted line) are plotted for comparison.

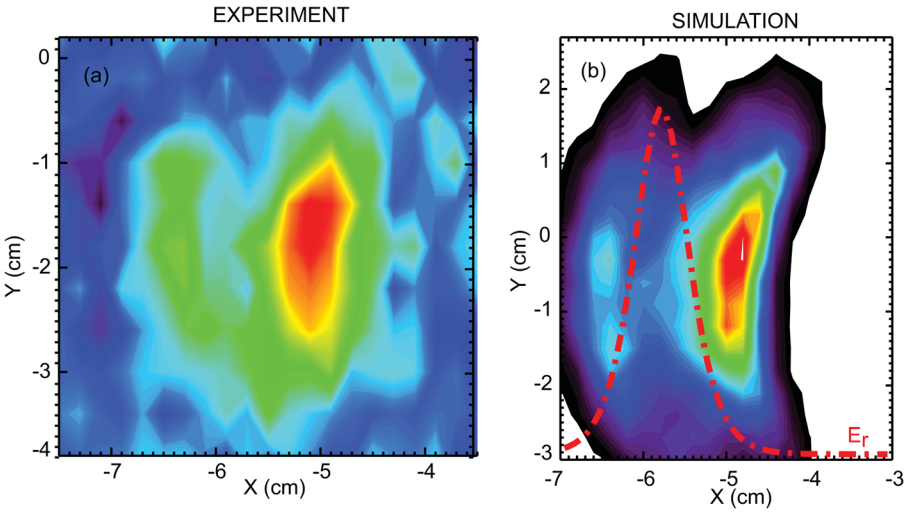

FIG. 12. Beam split observed in experiment (a) and in simulation (b). The split of the beam is correlated with a sharp gradient in plasma potential and misalignment of the beam relative to the potential fields.

fields. The radial drift and broadening of 50 000 test particles are evaluated. Furthermore, since the misalignment between the fast ion beam orbit and the annular obstacle can also modify the effect of the radial fields, a sensitivity study is conducted to quantify the effect of the static fields under several conditions with the beam orbit misaligned with the inner edge of the obstacle.

The beam profiles collected at 1–6 cyclotrons are shown in Fig. 10. A radial convective drift of the beam center is clearly shown in the simulation, with a typical value of ~1 cm after 6 gyrations. This is consistent with the amount of drift observed in the experiment. Note that the decrease in total number of particles in the simulation is mainly due to azimuthal spreading of the beam. (The simulation includes the instrument function of the collector, so ions that drift outside of the collector acceptance angle are considered lost.) The broadening of the ion beam FWHMs in these cases is evaluated in Fig. 11. The beam $FWHM^2$s are plotted against the number of beam gyrations. The red dashed line indicates the classical diffusion level of the beam in neon plasmas, and the red triangles shows the observed beam $FWHM^2$ in experiment with large turbulent waves present. The diamond symbols represent a case with the fast ion orbit well aligned with the obstacle ("centered"), and four cases with them misaligned by ±5 mm in either the x or y direction. The simulation shows that the static radial fields contribute to the broadening of the beam FWHM. However, wave-induced transport is still the dominant effect in the experimentally observed broadening of the fast-ion beam.

With higher bias (≥100 V) on the annular obstacle, the collected beams usually drift more radially and are degraded substantially, so that a quantitative measurement of the beam radial FWHM is difficult. Specifically, in cases with high V_{bias} and poor alignment between the beam orbit and the obstacle, a "split" of the collected beam profile is usually observed. Figure 12(a) shows a typical "split" beam profile, observed at 100 V obstacle-bias in neon plasmas. The split of the beam profile is mainly induced by the overlap of the beam with the peak of the radial electric field profile. Splitting of the beam profile is also observed in Monte Carlo simulations. Figure 12(b) shows a typical simulation result for a potential profile with sharp gradient. The radial electric field is plotted in dashed-dotted lines, and the initial beam is misaligned with the E_r fields by 5 mm. A "split" beam profile similar to the experimental one is observed.

The drift of the ion beam due to the static electric fields is unfavorable for studying the wave-induced, diffusive transport of the ion beam. Running the ion beam with a smaller gyro-radius to avoid the large plasma potential gradient regime is a possible method to minimize this effect. However, the gyro-radius of the beam has to be carefully chosen so that the beam trajectories are still able to overlap well with the mode structures of the waves.

VI. CONCLUSION

In the work described in this paper, the thermal plasma cross-field transport induced by electrostatic instabilities has been explored. The interaction between a test-particle fast-ion beam and the electrostatic wave turbulence has also been fully studied. The thermal plasma transport is affected by the sheared E × B flow at the plasma edge, and the overlap between density and potential fluctuation structures determines the radial confinement of the plasma density. The scaling of the fast ion transport in turbulent waves is well explained by gyro-averaging effects. And the time evolution of the fast ion beam width in waves is also consistent with diffusion theory.

Static electric fields cause both convective motion and broadening of the beam spot. The broadening of the spot is usually negligible compared to fluctuation-induced broadening but can be appreciable in the presence of sharp gradients in the electric field.

Several extensions of these studies are of interest. For example, the transport of both thermal plasma and energetic ions differs for electromagnetic and electrostatic fluctuations. Similar studies in plasmas with large magnetic fluctuations (e. g., drift-Alfvén waves) are feasible and promising.

ACKNOWLEDGMENTS

The authors gratefully acknowledge the assistance of Marvin Drandell, Zoltan Lucky, Patrick Prybil, Brett Friedman, David Schaffner, and Walter Gekelman for the experiment and

helpful discussions. This work was supported by DOE and performed at the UCLA BaPSF basic plasma user facility supported by the NSF/DOE.

[1]F. Wagner, G. Becker, K. Behringer, D. Campbell, A. Eberhagen, W. Engelhardt, G. Fussmann, O. Gehre, J. Gernhardt, G. v. Gierke, G. Haas, M. Huang, F. Karger, M. Keilhacker, O. Klüber, M. Kornherr, K. Lackner, G. Lisitano, G. G. Lister, H. M. Mayer, D. Meisel, E. R. Müller, H. Murmann, H. Niedermeyer, W. Poschenrieder, H. Rapp, H. Röhr, F. Schneider, G. Siller, E. Speth, A. Stäbler, K. H. Steuer, G. Venus, O. Vollmer, and Z. Yü, Phys. Rev. Lett. **49**, 1408 (1982).
[2]P. H. Diamond, S. I. Itoh, K. Itoh, and T. S. Hahm, Plasma Phys. Controlled Fusion **47**, R35 (2005).
[3]K. H. Burrell, Phys. Plasmas **4**, 1499 (1997).
[4]R. McWilliams and D. Edrich, Contrib. Plasma Phys. **46**, 411 (2006).
[5]R. J. Taylor, M. L. Brown, B. D. Fried, H. Grote, J. R. Liberati, G. J. Morales, P. Pribyl, D. Darrow, and M. Ono, Phys. Rev. Lett. **63**, 2365 (1989).
[6]R. R. Weynants, G. v. Oost, G. Bertschinger, J. Boedo, P. Brys, T. Delvigne, K. H. Dippel, F. Durodie, H. Euringer, K. H. Finken, D. S. Gray, J. D. Hey, D. L. Hillis, J. T. Hogan, L. Konen, R. Leners, A. M. Messiaen, A. Pospieszczyck, U. Samm, R. P. Schorn, B. Schweer, G. Telesca, R. v. Nieuwenhove, and P. E. Vandenplas, Nucl. Fusion **32**, 837 (1992).
[7]J. A. C. Cabral, C. A. F. Varandas, M. P. Alonso, P. Belo, R. Canário, H. Fernandes, R. Gomes, A. Malaquias, P. Malinov, F. Serra, F. Silva, and A. Soares, Plasma Phys. Controlled Fusion **40**, 1001 (1998).
[8]G. V. Oost, J. Adámek, V. Antoni, P. Balan, J. A. Boedo, P. Devynck, I. Ďuran, L. Eliseev, J. P. Gunn, M. Hron, C. Ionita, S. Jachmich, G. S. Kirnev, E. Martines, A. Melnikov, R. Schrittwieser, C. Silva, J. Stöckel, M. Tendler, C. Varandas, M. V. Schoor, V. Vershkov, and R. R. Weynants, Plasma Phys. Controlled Fusion **45**, 621 (2003).
[9]T. A. Carter and J. E. Maggs, Phys. Plasmas **16**, 012304 (2009).
[10]W. W. Heidbrink and G. Sadler, Nucl. Fusion **34**, 535 (1994).
[11]W. W. Heidbrink, J. M. Park, M. Murakami, C. C. Petty, C. Holcomb, and M. A. V. Zeeland, Phys. Rev. Lett. **103**, 175001 (2009).
[12]S. Günter, G. Conway, S. daGraça, H.-U. Fahrbach, C. F. M. G. Muñoz, and T. Hauff, Nucl. Fusion **47**, 920 (2007).
[13]T. Suzuki, S. Ide, T. Oikawa, T. Fujita, M. Ishikawa, and the JT-60 team, Nucl. Fusion **48**, 045002 (2008).
[14]J. M. McChesney, R. A. Stern, and P. M. Bellan, Phys. Rev. Lett. **59**, 1436 (1987).
[15]J. M. McChesney, P. M. Bellan, and R. A. Stern, Phys. Fluids B **3**, 3363 (1991).
[16]R. McWilliams, M. K. Okubo, and N. S. Wolf, Phys. Fluids B **2**, 523 (1990).
[17]J. Bowles, R. McWilliams, and N. Rynn, Phys. Rev. Lett. **68**, 1144 (1992).
[18]W. Zhang, Z. Lin, and L. Chen, Phys. Rev. Lett. **101**, 095001 (2008).
[19]T. Hauff and F. Jenko, Phys. Plasmas **13**, 102309 (2006).
[20]W. Gekelman, H. Pfister, Z. Lucky, J. Bamber, D. Leneman, and J. Maggs, Rev. Sci. Instrum. **62**, 2875 (1991).
[21]Y. Zhang, H. Boehmer, W. W. Heidbrink, and R. McWilliams, Rev. Sci. Instrum. **78**, 013302 (2007).
[22]S. Zhou, W. W. Heidbrink, H. Boehmer, R. McWilliams, T. A. Carter, S. Vincena, and B. Friedman, Phys. Plasmas **19**, 012116 (2012).
[23]S. Zhou, W. W. Heidbrink, H. Boehmer, R. McWilliams, T. A. Carter, S. Vincena, S. K. P. Tripathi, P. Popovich, B. Friedman, and F. Jenko, Phys. Plasmas **17**, 092103 (2010).
[24]S. Zhou, W. W. Heidbrink, H. Boehmer, R. McWilliams, T. A. Carter, S. Vincena, and S. K. P. Tripathi, Phys. Plasmas **18**, 082104 (2011).
[25]S. L. Chen and T. Sekiguchi, J. Appl. Phys. **36**, 2363 (1965).
[26]T. A. Carter, Phys. Plasmas **13**, 010701 (2006).